Defence Science Journal, Vol 47, No 4, October 1997, pp. 517-536


*REVIEW PAPER*

# Synthetic Aperture Radar: A Focus on Current Problems

M.S. Ranga Rao
*Defence Research & Development Laboratory, Hyderabad-500 258.*

and

P.R. Mahapatra
*Indian Institute of Science, Bangalore-560 012.*

**ABSTRACT**

Synthetic aperture radar (SAR) is a powerful tool for mapping and remote sensing. The theory and operation of SAR have seen a period of intense activity in recent years. This paper attempts to review some of the more advanced topics studied in connection with modern SAR systems based on digital processing. Following a brief review of the principles involved in the operation of SAR, attention is focussed on special topics such as advanced SAR modelling and focussing techniques, in particular clutterlock and autofocus, Doppler centroid (DC) estimation methods involving seismic migration technique, moving target imaging, bistatic radar imaging, effects of system nonlinearities, etc.

## 1. INTRODUCTION

Imaging radar systems are extremely useful surveillance tools for both civil and military applications. Their primary advantage is that they are able to provide all-weather, day-and-night coverage of earth's surface. Imaging can be performed by two classes of radar: real aperture radar (RAR) and synthetic aperture radar (SAR).

One of the most important parameters of a radar in relation to imaging is its resolution. A simple airborne radar can achieve significant resolution along the range direction (i.e., the radial direction projected on the ground) by employing a suitably narrow transmitted pulse. To achieve very fine resolution in this direction, it may even employ pulse compression. However, in a direction normal to the radial (called the azimuth direction), image resolution would be limited by the width of the antenna footprint. A radar operating in this mode is called RAR.

As the size of the antennas carried onboard aircraft and satellites is limited, azimuth resolution of the RAR is not high, and it gets progressively reduced at longer ranges. To overcome this limitation, the SAR principle was devised, which uses the incremental Doppler shift caused by adjacent points on the ground to enhance resolution.

The principal advantage of SAR over RAR is that the former can provide a much finer azimuth

Received 18 December 1995; revised 23 April 1997

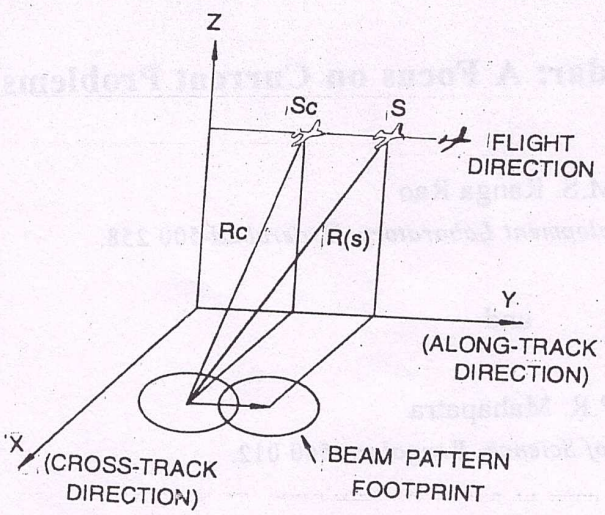


**Figure 1. Stripmap imaging geometry**

resolution than the latter, and the resolution can be kept uniform over the entire imaging area irrespective of the distance from the radar. For this reason, the SAR is a highly preferred imaging device in many applications[1-9]. This paper presents a brief description of the working principle of SAR, and concentrates on the special problem areas and their solution approaches.

## 2. WORKING PRINCIPLE OF SYNTHETIC APERTURE RADAR

The SAR is a fully coherent radar which processes the complex radar returns (consisting of amplitude and phase information) to achieve a much higher resolution than what is possible with the basic pattern of its antenna. The mapping geometry of a conventional strip-mapping SAR is shown in Fig. 1.

The SAR operates best when carried on a vehicle moving with constant velocity $V$ along a straight line path at constant altitude. In Fig. 1, the swath width of mapping corresponds to the ground range extent of the region illuminated by the antenna beam. The SAR antenna emits pulses of duration $\tau_p$ at regular intervals called pulse repetition time (PRT), the inverse of which is the pulse repetition frequency (PRF).

The SAR produces a two-dimensional ima
In the range direction (usually perpendicular to
direction of flight) image points are located by
round-trip time between the radiated and
received signals. In the along-track directio
scanning is done by the forward movement of t
antenna carried on the platform. Range resoluti
in SAR is obtained in a manner similar to that
RAR, either by employing a narrow transmitte
pulse or by pulse compression. The azimuth
along-track resolution is obtained by recording th
Doppler frequency of scattering elements in eac
of the range gates as they pass through the antenn
beam, and then performing a second puls
compression operation.

### 2.1 Synthetic Aperture Radar Data Acquisition

A simplified block diagram of SAR is shown in Fig. 2. A coherent waveform generator provides the chirp signal for transmission at the required PRF. The motion compensation unit helps stabilise the spatial orientation of the antenna and compensates for unforeseen platform velocity changes during the imaging period using information from the platform's inertial navigation system (INS). The coherent receiver converts the returns to baseband frequency for analog-to-digital (A/D) conversion. An azimuth presummer is usually employed to band-limit the data in the azimuth direction to the minimum Doppler bandwidth required for obtaining the desired azimuth resolution. The data is further processed for digital image formation.

### 2.2 Image Formation Algorithm

The radar receiver voltage phasor $a_r(R)$ is related to the complex terrain reflectivity $\sigma(R')$ of a given elemental area $dA'$ at range $R'$ as[4]

$$a_r(R) = \int_{-\infty}^{\infty} h(R \mid R')\, \sigma(R')\, dA' \qquad (1)$$

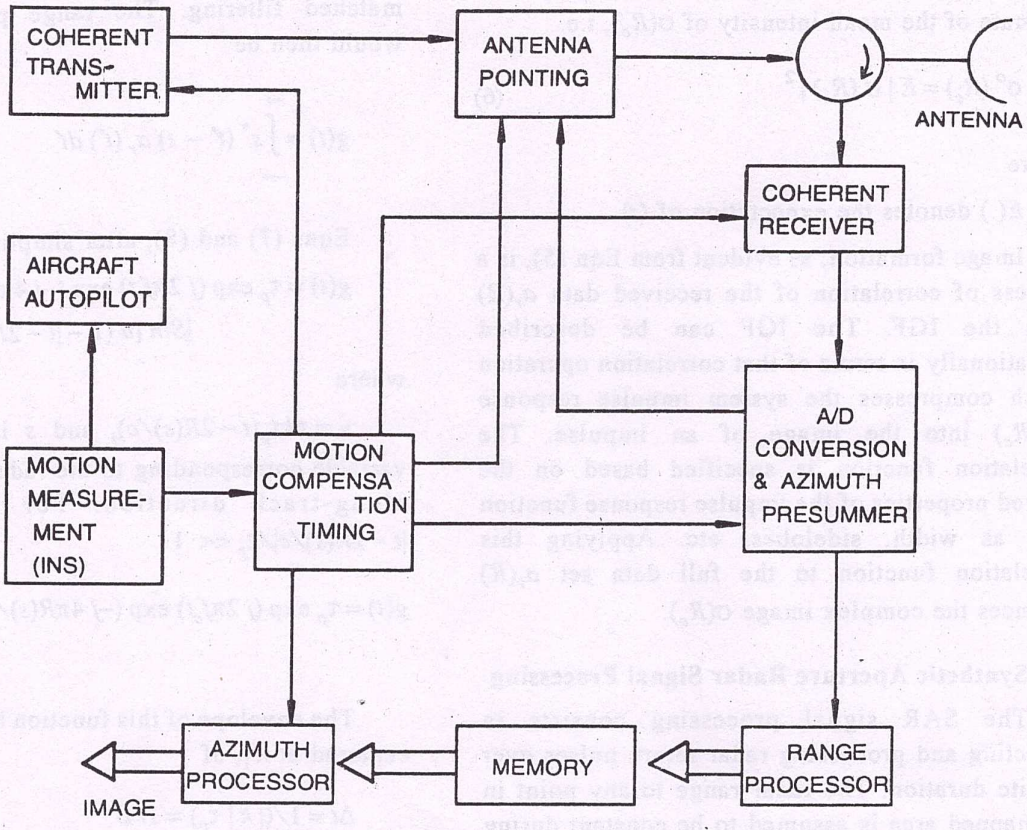


**Figure 2. Typical stripmap mode synthetic aperture radar system**

where

the integral is an area integral. The two-dimensional Green's function (impulse response) $h(R \mid R')$ is of the form

$$h(R \mid R') = K \exp[-j\, 4\pi|R - R'|/\lambda]/|R-R'|^2 \qquad (2)$$

where

$K$ is constant. The inverse Green's function (IGF) $h^{-1}(R_c|R)$ is given by the relation

$$\int_{-\infty}^{\infty} h^{-1}(R_c \mid R)\, h(R \mid R')\, dR = \delta(R_c - R') \qquad (3)$$

where

the two-dimensional Dirac delta function $\delta(R - R')$ is defined by

$$\int_{-\infty}^{\infty} f(R')\, \delta(R - R')\, dR' = f(R) \qquad (4)$$

An image formation algorithm is then described, based on the above relations, as

$$\int_{-\infty}^{\infty} h^{-1}(R_c \mid R)\, a_r(R)\, dR = \sigma(R_c) \qquad (5)$$

where

$a_r(R)$ represents the complex received data phasor array, and $\sigma(R_c)$ represents the complex image function at an arbitrary point at range $R_c$. The reflectivity $\sigma(R_c)$ from Eqn (5) will represent the ground truth only insofar as the system resolution properties allow the Dirac delta function to be reconstructed from the impulse response. The

reflectivity $\sigma^o(R_c)$ of each image point is finally an estimate of the mean intensity of $\sigma(R_c)$, i.e.

$$\sigma^o(R_c) = E\,|\,\sigma(R_c)\,|^2 \qquad (6)$$

where

$E(.)$ denotes the expectation of $(.)$.

Image formation, as evident from Eqn (5), is a process of correlation of the received data $a_r(R)$ with the IGF. The IGF can be described operationally in terms of that correlation operation which compresses the system impulse response $h(R|R_c)$ into the image of an impulse. The correlation function is specified based on the desired properties of the impulse response function such as width, sidelobes, etc. Applying this correlation function to the full data set $a_r(R)$ produces the complex image $\sigma(R_c)$.

### 2.3 Synthetic Aperture Radar Signal Processing

The SAR signal processing consists in collecting and processing radar return pulses over a finite duration. The radar range to any point in the mapped area is assumed to be constant during the pulse width, i.e. the effect of platform motion during one transmitted pulse width is neglected. This permits independent processing of the raw radar data in range and azimuth directions. The data is first compressed across all range resolution cells and then across the azimuth resolution cells[4,6-8].

#### *2.3.1 Range Processing*

Consider the imaging geometry shown in Fig. 1, with the radar transmitting a narrow-band linear frequency modulated (FM) signal. The transmitted chirp signal $s(t)$ is given as

$$s(t) = \exp\,[j\,2\pi\,(f_c t + kt^2/2)] \qquad |\,t\,| < \tau_p \qquad (7)$$

where

$f_c$ is the carrier frequency and $k$ is the chirp constant, i.e. the frequency sweep rate. The received signal is then compressed by correlating it with delayed versions of the complex conjugate signal $s^*(t)$. This correlation is equivalent to matched filtering. The range processor output would then be

$$g(t) = \int_{-\infty}^{\infty} s^*(t' - t)\, a_r(t')\, dt' \qquad (8)$$

Eqns (7) and (8), after simplification, yield

$$g(t) = \tau_p \exp(j\,2\pi f_c t) \exp(-j\,4\pi R(s)/\lambda) \times \{Sin\,[u\,(1 - |t - 2R(s)/c|/\tau_p)]\}/u$$

where

$u = \pi k \tau_p (t - 2R(s)/c)$, and $s$ is the slow-time variable corresponding to the radar position in the along-track direction. For the condition $|t - 2R(s)/c|/\tau_p << 1$

$$g(t) = \tau_p \exp(j\,2\pi f_c t) \exp(-j\,4\pi R(s)/\lambda)\,[Sin\,(u)]/u \qquad (9)$$

The envelope of this function has a 3 dB width, centered at $R_1$, of

$$\Delta t = 1/(|\,k\,|\,\tau_p) = 1/B \qquad (10)$$

where

$B$ is the signal bandwidth, corresponding to a slant range resolution of $\Delta R = c/2B$, and yielding a ground range resolution of $\Delta R_x = c/(2B\,Cos\alpha)$, where $\alpha$ is the look-down angle. The coarse ground range resolution without pulse compression is $\Delta R_x = c\tau_p/(2\,Cos\alpha)$.

#### *2.3.2 Azimuth Processing*

Azimuth compression is performed through a correlation process. The reference waveform $h^{-1}$ for correlation depends on the point in the image being processed. The range-compressed data as given by Eqn (8), suppressing the carrier, is

$$g(s/x_c, R_c) = \exp\,[-j\,4\pi R\,(s)/\lambda] \qquad (11)$$

The complex image function is obtained by the following process:

$$\sigma(R_c) = \int_{s_c - S/2}^{s_c + s/2} h^{-1}(s - s', R_c)\, g(s, R_c)\, ds \qquad (12)$$

This algorithm is the conventional time domain correlation algorithm. A good computational efficiency can be achieved if frequency domain techniques are exploited to implement this correlation operation.

*2.3.2.1 Azimuth Correlator Function*

The two-way phase shift of the signal received by the radar at an instant $s$ (measured along-track) is

$$\Phi = -4\pi R(s)/\lambda \qquad (13)$$

The slant range $R(s)$, expressed in terms of the vehicle velocity, is given by the relation

$$R^2(s) = R_c^2 + (s - s_c)^2 \qquad (14a)$$

Since the second term of the RHS is usually much smaller than the first, the following approximation is valid:

$$R(s) = R_c + \frac{V^2 s^2}{2 R_c} \qquad (14b)$$

From Eqns (13) and (14b), the phase change is

$$\Phi = \frac{-2\pi V^2 s^2}{\lambda R_c} \qquad (15)$$

The Doppler frequency is obtained by differentiating Eqn (15)

$$f_D = d\Phi/ds = -2V^2 s/\lambda R_c \qquad (16)$$

The rate of change of Doppler frequency is

$$f_R = -2V^2/\lambda R_c \qquad (17)$$

Expanding Eqn (14b)) using Taylor's series around $R_c$ gives

$$R(s) = R_c + \dot{R}_c (s - s_c) + \ddot{R}_c (s - s_c)^2 + \ldots\ldots \qquad (18)$$

where

$R_c$ is the range to the image point under consideration, and $\dot{R}_c$ and $\ddot{R}_c$ are respectively the first and second derivatives with respect to the slow time $s$. The Doppler frequency $f_D$ consists of two parts: the Doppler centroid (DC) $f_{DC}$ and the Doppler rate $f_R$. The second term in Eqn (18) corresponds to the DC $f_{DC}$ and the third term corresponds to the Doppler rate $f_R$. Hence

$$f_{DC} = -2\dot{R}(s)/\lambda \qquad (19)$$

$$f_R = -2\ddot{R}(s)/\lambda \qquad (20)$$

Combining Eqns (11) and (18), and using Eqns (19) and (20), the range compressed echo is given as

$$g(t_s, R_c) = \exp(-j\, 4\pi R_c/\lambda) \times \exp[j\, 2\pi f_{DC}(s - s_c) + f_R (s - s_c)^2/2] \qquad (21)$$

This is a linear FM waveform with centre frequency $f_{DC}$ and frequency sweep rate $f_R$. The azimuth correlation operation can then be realised approximately using a correlator function

$$h^{-1}(s, R_c) = \exp[-j\, 2\pi (f_{DC} s^2 + f_R s^2/2)] \qquad (22)$$

The complex image function is given by

$$\sigma(s_c', R_c) = T\,|\,[Sin(u)]/u\,| \qquad (23)$$

where

$u = \pi f_R s\,(s_c' - s_c)$ and $T$ is the target illumination time or SAR integration time. The nominal width of the pulse is

$$\delta s = 1/B_D$$

where

$B_D = |f_R|\,T$ is the Doppler bandwidth. The spatial resolution in the azimuth direction corresponding to the Doppler bandwidth $B_D$ is

$$R_y = V\delta s = V/B_D$$

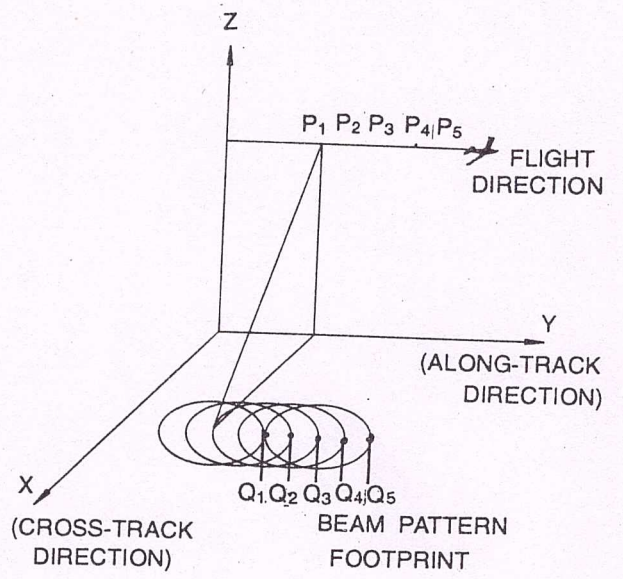


**Figure 3(a). Effect of radar motion on returns from scatterers: geometry of scanning of successive point scatterers by motion of radar platform.**

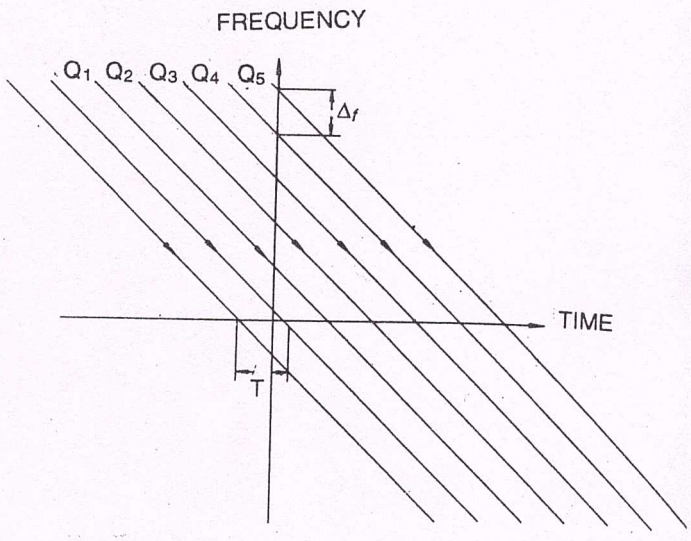


**Figure 3(b). Effect of radar motion on returns from scatterers: the resultant.**

$$= V/(|f_R|T) \tag{24}$$

The resolution is independent of the radar range and is inversely proportional to the processor bandwidth. Hence, an image with a finer azimuth resolution can be obtained by collecting the data over a longer duration of time, thus generating a longer synthetic aperture.

*2.3.2.2 Integration Time*

From Eqn (16), it is clear that the Doppler frequency of the returns from the point targets in a given range gate varies linearly as the radar platform moves forward. Consider Fig. 3(a) in which are shown five different points $Q_1$ .... $Q_5$ all on a line parallel to the platform motion. The points successively enter and leave the 3 dB beamwidth as the radar platform moves through positions $P_1$ ... $P_5$.

The Doppler variation of these points is observed to be identical, except for a constant time shift (Fig. 3(b)). This time shift is equal to the time the radar platform would need to traverse the along-track distance between two adjacent ground points. Two types of processing are possible depending on the desired resolution.

*(a) Unfocussed Processing*

Integration of pulses is performed over an interval of time $T$, before the two-way phase of the return pulses change by $\pi/2$ radians. This condition ensures that all the returns within the integration time contribute constructively to the integral. Substituting $\Phi = \pi/4$ and $s = T/2$ in Eqn (15), we obtain

$$VT = \frac{\sqrt{\lambda R_c}}{\sqrt{2}} \tag{25}$$

Combining Eqns (17) and (25) by eliminating $f_R$, we get

$$\Delta R_y = \frac{V}{2V^2T/\lambda R_c} \tag{26}$$

Further, combining Eqns (25) and (26) by eliminating $V$ and $T$, we get the azimuth resolution $\Delta R_y$ for the unfocussed case as

$$\Delta R_y = \frac{R_c\lambda}{2(\sqrt{\lambda R_c/2})} = \frac{\sqrt{\lambda R_c}}{\sqrt{2}} \tag{27}$$

This resolution is dependent on the radar range, and gives a coarser resolution at longer ranges. However, it is desirable that the picture resolution be independent of the radar range. Hence, focused processing techniques, which have the property of range-independent resolution, are preferred for SAR imaging.

*(b) Focussed Processing*

Equation (14b), neglecting the higher order terms and correcting the phase of the radar returns by an amount specified by Eqn (15), allows a longer coherent integration time than the unfocussed processing case. This results in finer frequency resolution and hence finer azimuth resolution. For focused processing, integration is done over a time $T$ during which the radar travels past the entire 3 dB width. This time duration $T$ is easily seen to be

$$T = \frac{\lambda R_c}{L_a V} \tag{28}$$

The Doppler bandwidth $B_D$ in this interval $T$ is obtained from Eqn (16) as

$$B_D = \left(\frac{2V^2}{\lambda R_c}\right)\left(\frac{\lambda R_c}{L_a V}\right) = \frac{2V}{L_a} \tag{29}$$

Combining Eqns (24) and (29), we get

$$\Delta R_y = L_a/2 \tag{30}$$

This result shows that the azimuth resolution of an ideal focused SAR is independent of the range from the radar, and is equal to half of the antenna dimension. In actual implementation, this relationship cannot be stretched to the extreme to obtain arbitrarily fine resolution from considerations of radiated power and signal-to-noise ratio (SNR). However, resolution of the order of a few metres can be obtained using focused processing.

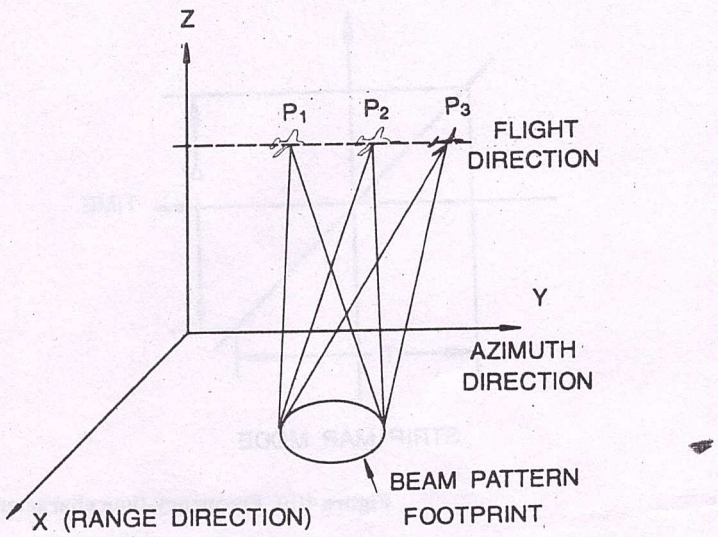


**Figure 4(a). Spotlight mode synthetic aperture radar imaging geometry.**

## 3. DIFFERENT TYPES OF SYNTHETIC APERTURE RADAR

Depending on the nature of application, synthetic aperture radar imaging is classified into the following:

### 3.1 Stripmapping Mode Synthetic Aperture Radar

The conventional mode of SAR imaging is based on the stripmap SAR processing. This mode is used for mapping large strips of terrain, as shown in Fig. 1. The theory of imaging reviewed in Section 2 is directly relevant to the stripmap mode of SAR operation.

### 3.2 Spotlight Mode Synthetic Aperture Radar

In the conventional strip-map mode of imaging, the ground resolution along the direction of platform motion is limited by the integration time, which is decided by the flight time of the platform over the along-track width of the antenna footprint. To achieve a finer resolution, SAR may be operated in the spotlight mode[7] (Fig. 4(a)) in which the antenna boresight is continually realigned so as to point to the centre of the scene even as the platform moves past the area being mapped. Obviously, the enhanced resolution in the

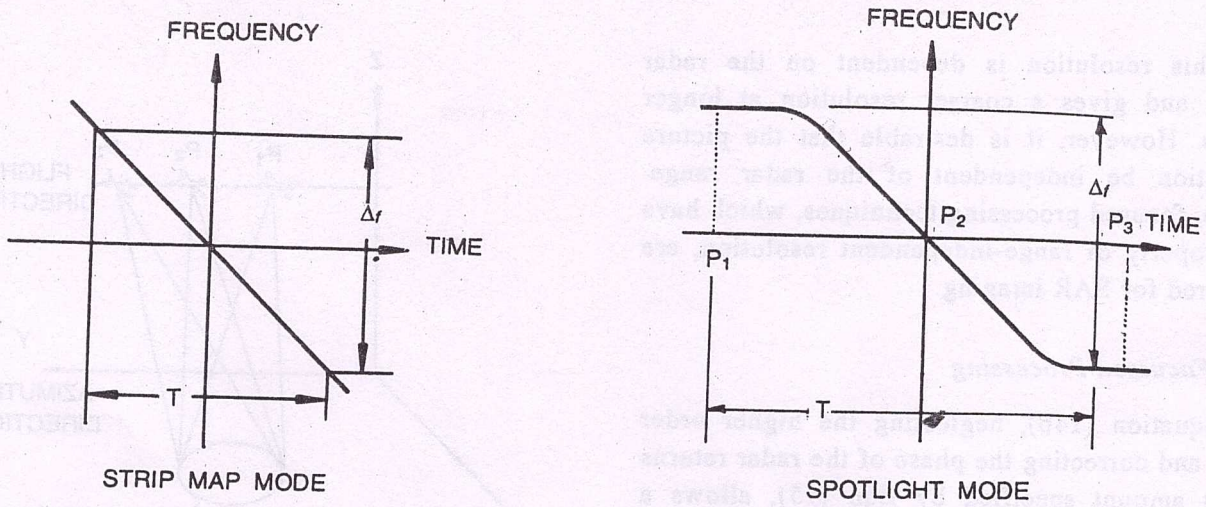


**Figure 4(b). Frequency-time characteristics of stripmap and spotlight modes**

spotlight mode is obtained at the expense of a lower imaging area than in the strip-map mode.

The antenna beamwidth in the spotlight mode must be large enough to adequately illuminate the area to be imaged, and the duration of the illumination (and integration) must be long enough to obtain sufficient effective rotation of the scene to yield the desired along-track resolution. The long period of scene observation and signal integration, however, means that the Doppler history from a fixed point on the ground may show significant nonlinearity, unlike the strip-map operation in which observation over narrow angles ensures linearity of the Doppler return as a function of time. This comparison is shown in Fig. 4(b). The processor used for signal compression has to take care of such nonlinearity. A motion-sensing system, such as the vehicle's inertial navigation system (INS) is used to determine the required antenna pointing angles and to provide knowledge of the relative motion between the vehicle and the scene. The increase in range during the relatively large illumination time is compensated using INS-derived information.

### 3.3 Spotlight Mapping

A major drawback of the normal stripmap mode radar is the requirement of relatively large integration time, usually of the order of a second or more, for image generation. This problem is worse with the spotlight mode. Further, these two modes of SAR operation are highly processing-intensive. In some applications where lower imaging and processing time is demanded, a form of imaging called spotlight mapping is used. In the spotlight mapping[5], resolution along the track is obtained by a direct bandpass filtering of the composite return from each range gate. The antenna beam may or may not be squinted. Figure 5 shows the imaging geometry and the Doppler frequency returns from different point scatterers in a range gate within the beam. The Doppler variation along a given range strip will be linear for small beam widths. The processing involves deramping the signal using a local oscillator with the same frequency slope as that of the Doppler return. This keeps the Doppler frequency of the signal output for each scatterer constant during the imaging period. The signal corresponding to each pixel is then resolved in azimuth by using spectral analysis techniques, such as the discrete Fourier transform (DFT). Since the phase is compensated partially, it can be considered as a partially focused synthetic aperture map.

Spotlight mapping is generally used in multifunction array radars (MFAR) which perform

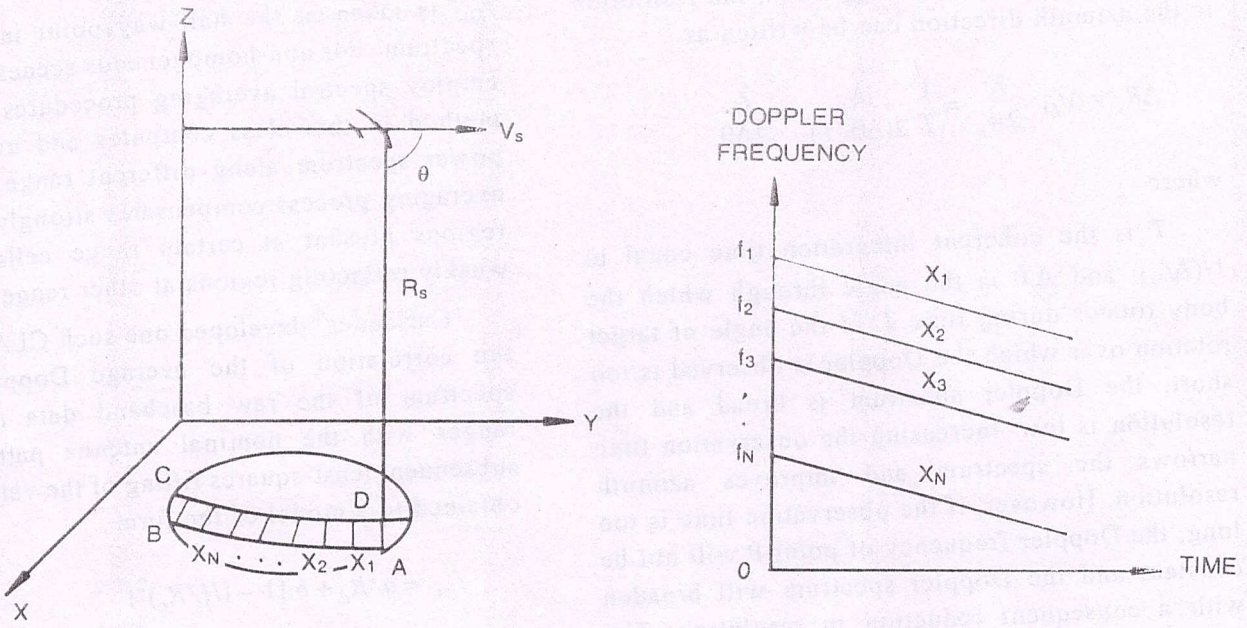


**Figure 5. Spotlight mapping**

other functions, such as air-to-air search and track, and terrain-following and avoidance. Such radars share their computational resources among many functions, and are typically carried on manoeuvering aircraft which allow very short time for imaging. One application of spotlight imagery in such aircraft is to update the navigation system by locating known landmarks. Another application is in weapon targeting and delivery.

### 3.4 Inverse Synthetic Aperture Radar

Unlike the normal SAR where the radar is moved relative to the stationary platform, in inverse SAR (ISAR), the target is imaged by a stationary radar using the Doppler information due to the motion of the target. ISAR is most beneficially used in mapping of rotating targets. In fact, the earliest use of the SAR class of principles was made for the mapping of the moon and the planet Venus using the ISAR principle. More tactical uses of the technique concern the imaging of manoeuvring aircraft and ships.

A rigid body rotating at an angular speed $w_r$ rad/s, with the axis of rotation normal to the plane of the paper, is shown in Fig. 6. The Doppler shift caused by a point on the body at a distance $r$ from the axis of rotation is[1]

$$f_D = \frac{2v\cos\alpha}{\lambda} = \frac{2w_r r\cos\alpha}{\lambda} = \frac{2w_r y}{\lambda}$$

where

$v$ is velocity of the point P, and it makes an angle $\alpha$ with the line-of-sight (LOS) from the radar

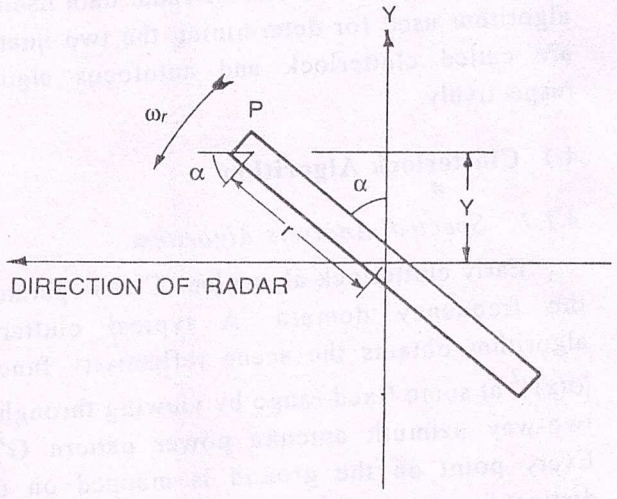


**Figure 6. Inverse synthetic aperture radar**

to the point P. Using this equation, the resolution in the azimuth direction can be written as

$$\Delta R_y = \Delta f_D \frac{\lambda}{2w_r} = \frac{1}{T}\frac{\lambda}{2(\Delta\theta/T)} = \frac{\lambda}{2\Delta\theta}$$

where

$T$ is the coherent integration time equal to $1/(\Delta f_D)$, and $\Delta\theta$ is the angle through which the body rotates during time $T$. If the angle of target rotation over which the Doppler is observed is too short, the Doppler spectrum is broad and the resolution is low. Increasing the observation time narrows the spectrum and improves azimuth resolution. However, if the observation time is too long, the Doppler frequency of point P will not be constant and the Doppler spectrum will broaden with a consequent reduction in resolution. The result is that there will be an optimum time of observation to image a target with the inverse SAR technique.

## 4. CLUTTERLOCK & AUTOFOCUS

For azimuth compression using correlation function (Eqn (22)), a knowledge of $f_{DC}$ and $f_R$ is required. These quantities are usually obtained from platform motion measuring devices (such as inertial measuring units) which are fairly accurate. However, for high quality images, most image formation algorithm perform automatic determination of the DC $f_{DC}$ and the Doppler rate $f_R$ using information derived from the radar data itself. The algorithm used for determining the two quantities are called clutterlock and autofocus algorithm respectively.

### 4.1 Clutterlock Algorithm

#### *4.1.1 Spectral Analysis Algorithm*

Early clutterlock algorithm (CLA) operated in the frequency domain. A typical clutterlock algorithm obtains the scene reflectivity function $|\sigma(x)|^2$ at some fixed range by viewing through the two-way azimuth antenna power pattern $G^2(x)$. Every point on the ground is mapped on to a distinct frequency point. For a homogeneous scene, $f_{DC}$ is taken at the half-way point in the pow spectrum. For non-homogeneous scenes, the CL employ spectral averaging procedures. A typi method in this class computes and averages t power spectrum along different range lines. T averaging process compensates strongly reflecti regions present at certain range cells with t weakly reflecting regions at other range cells.

Curlander[4] developed one such CLA based the correlation of the average Doppler pow spectrum of the raw baseband data at variou ranges with the nominal antenna pattern, wit subsequent least-squares fitting of the values of $f_D$ obtained to a model of the form

$$f_{DC} = a/R_c + b\,[1 - (H/R_c)^2]^{1/2} \quad (31$$

The values of the constants $a$ and $b$ ar determined by choosing a cluster of adjacent range bins, and taking a fast Fourier transform (FFT) fo each of these range bins in the azimuth direction to create the Doppler spectra. The squared amplitudes of these adjacent Doppler spectra are averaged at each frequency to yield a single power spectrum for each cluster. Each averaged power spectrum is then correlated with the nominal two-way antenna power pattern $G^2(s)$ in the along-track direction to obtain an estimate of $f_{DC}(R_c)$ corresponding to the centre of that particular cluster. The values obtained for the various clusters across the full range swath are then fitted to the Doppler centroid model to determine the constants $a$ and $b$.

#### *4.1.2 Energy Balance Algorithm*

Nominal values of $f_{DC}$ and $f_R$ are usually obtained from the radar platform motion sensors. Curlander[11] considered four small real images of a four-look processor i.e. a processor that obtains four images of the same patch viewed at different aspect angles as the vehicle moves forward, and processed independently in different frequency bands. The images are obtained using $f_{DC}$ and $f_R$ values. Assumption of small images allows $f_{DC}$ to be constant over the image and the variations in reflectivity with aspect angle to be small. The total

energy $E_i$ in each of these four images is found by summing the pixel intensities over each image. For true value of $f_{DC}$, the sum of the energies in the two lower-frequency-look images and that in the two upper-frequency-look images must be equal. Through trial and error, the value of $f_{DC}$ for which the energy E equals zero is taken as the actual value for $f_{DC}$. Li *et al.*[12,13] developed an improved version of this algorithm in which a single full-aperture image is produced using a trial value $f_{DC}$ at each range. Azimuth spectra are produced and averaged over a number of adjacent range bins spanning a small region over which $f_{DC}(R)$ is nominally constant. Each average power spectrum is then balanced to find the frequency above and below which one half of the power lies. The estimates of $f_{DC}$ so obtained are fitted to a linear model to determine the final values of $f_{DC}(R)$.

#### *4.1.3 Minimum-Variance Unbiased Centroid Estimation*

Jin and Chang[4] (see Ch 5.3) have considered a CLA for homogeneous scenes for which the exponentially distributed intensities of the scene elements have constant mean, so that the backscatter coefficient $\sigma^o$ is constant. For such scenes, they derived an expression for the minimum-variance unbiased estimator $f_{DC}$ of the deviation of the Doppler frequency, used to form the image, from the true value of $f_{DC}$. In this algorithm, an estimate $\sigma^o$ of the mean image intensity is required.

#### *4.1.4 Clutterlock for a Quasi-Homogeneous Scene*

In this method[14], the image is divided into a number of subregions with equal mean intensity $\sigma^o$ over each subregion. The energy balance algorithm and the minimum-variance unbiased centroid estimation, respectively, are applied to find $E$ and $f_{DC}$ of each of these subregions. The resulting values of $f_{DC}$ are then combined in inverse proportion to their variances to produce a final value of $f_{DC}$ for the image as a whole.

#### *4.1.5 Time Domain Correlation*

Madsen[15] has developed a CLA which is based on the fact that the power spectral density $S(f)$ of a stationary random process such as the Fresnel reflectivity of the azimuth line is the Fourier transform of its autocorrelation function $R(\tau)$, i.e.

$$S(f) = \int_{-\infty}^{\infty} R(\tau) \exp(-j2\pi f\tau)\, d\tau$$

Any phase shift in the spatial domain results in a frequency shift in the transformed domain. Thus,

$$S(f - f_{DC}) \iff R(\tau) \exp(j2\pi f_{DC}\tau)$$

Using the above relationships, $f_{DC}$ is determined by analysing the phase of the slow time correlation function $R(\tau)$.

The methods of Doppler centroid estimation given in this section are representative, and not exhaustive. Other methods for DC estimation are given elsewhere[17,18].

### 4.2 Autofocus Algorithm

Most SAR image formation processors determine the $f_R$ using the subaperture correlation method. In the method developed by Curlander[11], two complete images are produced in different parts of the Doppler spectrum as in multilook processing. Their size is small enough in range extent that $f_R$ is considered constant, and large enough in azimuth extent to allow efficient FFT computation. The two images are obtained based on some trial value of the Doppler rate $f_R'$. Their separation in azimuth time is given by

$$s' = (f_{DC1} - f_{DC2})/f_R'$$

where

$f_{DC1}$, $f_{DC2}$ are the DC values used to form the images. For an exact value of Doppler rate $f_{R'}$ their separation would be

$$s = (f_{DC1} - f_{DC2})/f_R$$

The difference between $s'$ and $s$ gives a measure of the mismatch in $f_R$ between the scene and the processor outputs.

## 5. REAL EFFECTS ON SYNTHETIC APERTURE RADAR IMAGING

Several factors affect the performance of a SAR system. The nonlinearities of the SAR subsystems degrade the system resolution capabilities. The other sources of noise are the sensor position and velocity errors which result in geometric distortions in the image.

### 5.1 System Nonlinear Effects

SAR system performance is degraded by various noise sources. They include: (i) amplitude and phase errors which degrade the system impulse response function (IRF), (ii) Thermal noise degrading the system dynamic range, and (iii) distortion noise introduced by quantisation error, system nonlinearities and bit error noise, degrading the range and the azimuth IRF's.

### 5.2 Geometric Distortion

Geometric errors[4,19-21,30] in the image are produced due to errors in sensor parameters, platform motion and target location. Sensor errors such as oscillator long- and short-term stability result in along-track scale error. An error in the estimate of slant range resulting from electronic delay through the transmitter-receiver chain leads to incorrect across-track scale error. Further, Doppler shifts due to the earth's rotational velocity give rise to incorrect estimate of DC. This error results in a pixel location error proportional to the difference between the reference and the actual values of the DC. Platform motion (position and velocity) errors generate pixel location errors in both azimuth and range directions. Moreover, the velocity errors also result in azimuth scale errors in the image.

Three special types of geometric errors encountered in SAR imagery are referred to as foreshortening, layover, and shadowing. For rough surfaces, foreshortening occurs because of the slope of the local terrain. The apparent pi spacing in the range direction is different from actual spacing on the terrain. The layo phenomenon occurs for steep terrains, such mountain sides, which have an inclination grea than that of the radar wavefront at the location the feature. The echoes from pixels at farth across-track position arrive earlier in time th those from the pixels at close across-tra positions, causing an apparent layover. Tl shadowing effect is predominant for terrains slope steeper than the LOS from the radar to the poi being imaged. Points on such a slope are shielde from the radar, receiving no radiation and returnin no echo. The details on such shielded areas are therefore, lost much as in the case of optica shadow.

### 5.3 Range Migration

Range migration is an inevitable consequence of SAR operation. The azimuth resolution in SAR image formation depends on the width of the Doppler band. If the Doppler is to have a finite bandwidth, the range to the target must change during the illumination time, and as a consequence the compressed point target response necessarily occurs at different ranges for different pulses. The azimuth signal needed for compression processing is, therefore, assembled from slightly varying range resolution cells for different pulses within the integration interval, as given by Eqn (18). This is the phenomenon of range migration whose degrading effect is severe in the case of satellite-borne SAR systems (because of their high velocities), and which may be corrected employing secondary range compression methods[22-24]

Range migration consists of two parts: range walk and range curvature. These correspond respectively to the second and third terms on the RHS of Eqn (18).

### 5.4 Speckle Noise Effects

Speckle noise is inherent in the coherent nature of the radar signal itself. SAR processing involves estimation of the intensity level of each

image element using some realisation of a random process. The dimension of each image element is much greater than the radar wavelength, and hence the echo from the element is the complex sum interference of the backscattered electric fields from the multitudinous facets of the distributed scene. However, because of the random phase distribution of the incident radiation over the pixel area, the summation will contain a random component in the amplitude of the complex sum. The discrepancy between the true and observed values of the mean backscatter coefficient $\sigma^o$ for each element constitutes the speckle noise, and results in a mottled appearance of the SAR image of the terrain, which is nominally homogeneous. Speckle noise reducing methods are a subject of study[4,24]

## 6. ADVANCED TOPICS IN SYNTHETIC APERTURE RADAR PROCESSING

### 6.1 Doppler Centroid Migration

Because of the vertical component of the platform motion, which may be deliberate or due to inadvertent departures from the desired flight path, the centroid of the Doppler spectrum 'seen' by the SAR may not remain constant. When the DC shows rapid variations with range or azimuth, difficulties may be encountered in SAR processing. However, the computational efficiency of the frequency domain techniques can still be exploited by modifying the SAR raw data sampled at Nyquist rate, and then applying a space-varying one-dimensional filter to the focused image. Prati and Rocca[16] discussed a computationally efficient focusing, based on frequency domain techniques, which requires a knowledge of the DC. If the PRF is sufficiently high, the spectral folding can be ignored. The exact value of DC is not necessary for focusing, as the focusing operator is defined over the entire spectrum. Computation time is reduced by using the filtering effect of the antenna beam to limit the focusing to the received signal bandwidth. If the antenna pointing changes, a wider bandwidth is to be focused at the cost of computational efficiency. The azimuth data spectrum is folded many times, depending on the ratio between the actual value of the DC and the sampling rate.

Doppler centroid estimation errors generate an incorrectly reconstructed spectrum. The correct part of the Doppler history generates a point response at the correct position with degraded resolution. The folded part of the Doppler history generates a ghost image at a position corresponding to one PRF away from the main response. The relative intensity of ghost images is controlled by processing sub-blocks of azimuth data. To take advantage of frequency domain techniques, the processing bandwidth is expanded $N$ times by interleaving $N$-1 zeros between adjacent samples in azimuth. This correctly links the folded spectral replicas (ghosts) with unfolded ones (main responses). However, this method results in ghost images on either side of the scatterer under consideration that fill wavenumber bands which are separable from that of the actual image. Such a procedure avoids the need for the exact value of DC. This technique is applied whenever the DC variation is the limiting factor for the data block length of frequency domain processing techniques. Another application is that the spotlight SAR data can be processed by strip-map processing.

### 6.2 Advanced Focusing Techniques

Cafforio, *et al.*[26] proposed an efficient SAR focusing method based on range migration techniques used in geophysics. Conventional SAR focusing algorithm compensate for the defocusing occurring due to the range walk and range curvature part of range migration. The radiating reflector (RR) technique, used in geophysics for wave propagation, is applied in this method. Operation of the pulsed radar in motion is considered as the sampling of the radiated field at a set of points along the sensor trajectory (Fig. 7). It is assumed that all the point scatterers radiate simultaneously.

The field due to a distribution $i(y, z)$ of sources emitting at time $t = 0$, as measured along the sensor path, is

$$\Gamma(x = 0, y, r = 0, w) = \frac{1}{4\pi}\iint i(y', r') \frac{\exp[-jwt(y, y', r',)]}{R} dy'\, dr'$$

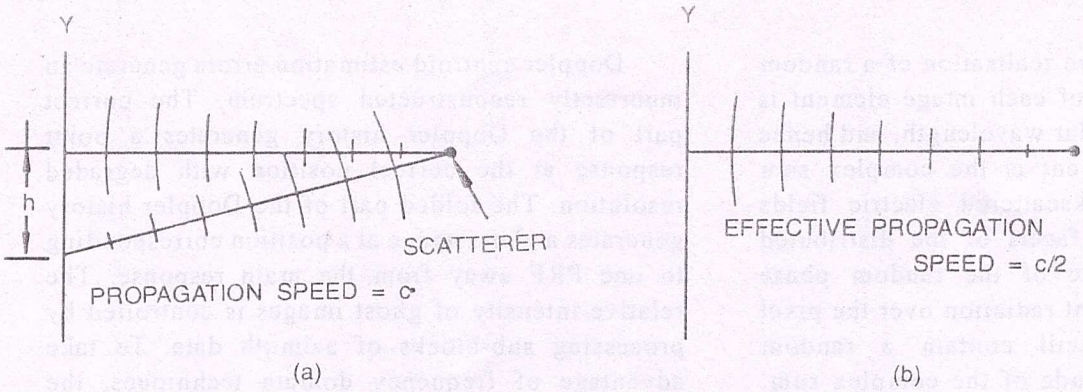


**Figure 7(a). Synthetic aperture radar imaging of a single scatterer in real situation and (b) its radiating reflector model**

where

$R = [x'^2 + (y - y')^2 + r'^2\, x]^{1/2}$ is the across-track coordinate, $y$ is the along-track coordinate, and $r$ is the distance in the imaginary plane containing the sensor trajectory and the point scatterers in a direction orthogonal to the $y$-direction. The inversion process to determine $i(y', r')$ consists of downward continuation of the wavefield along the $r$-axis, followed by determination of the amplitudes of the wavefield at the source locations at the time instant $t = 0$. The downward continuation involves decomposition of the field into monochromatic plane waves, and then applying proper values of phase rotation to each of these plane waves. Decomposition into plane waves involves computation of two-dimensional Fourier transform of the received data. The plane wave representation is given by

$$D(k_y, r = 0, w) = \iint d(y, r = 0, t) \exp[-j(wt + k_y y)]\, dy dt$$

The phase operator required to back-propagate from $r = 0$ (sensor) to $r = r_o$ (source) is $\Omega = k_r r_o$ and the corresponding back-propagation relation for the plane wave with wavenumber $k_y$ is

$$D(k_y, r, w) = D(k_y, r = 0, w) \exp[k_y r]$$

The measured field, considered to be produced by sources radiating at time $t = -t_o$, is

$$d(y, r, t = -t_0) = \int_{-w_s/2}^{w_s/2} dw \int_{k_{y\min}}^{k_{y\max}} D(k_y, r = 0, w) \exp[jk_y r] \exp[j\{K_y y + w(-t_o)\}]\, dk_y$$

This gives the complex reflectivity function at the source point. The double integral can be formulated into a two-dimensional Fourier transform to make use of efficient frequency domain techniques.

### 6.3 New Model for Synthetic Aperture Radar Imaging

Soumekh[27] developed a SAR/ISAR inverse method based on a source/object interaction system model that considers the spherical radiation pattern of the radar's signal as well as the wave scattered from a differential scatterer in the spatial domain. Figure 8 shows the imaging geometry. $(X_1, Y_1)$ represents the radar coordinates at the centre of the aperture. This method essentially consists in representing the radar's spherical waves in terms of plane waves travelling towards the synthesised aperture. Mathematically, the model utilises the spherical Hankel wave function in its integral form. This representation gives the following relationship between the complex reflectivity function and the received signal in the frequency domain:

$$F(k_x, k_y) = \exp(-jk_x X_1 - jk_y Y_1)\, S(k_u, w)$$

where

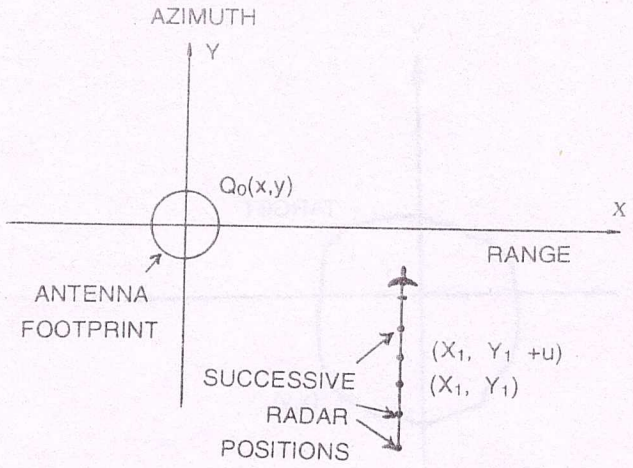


**Figure 8. Squint mode synthetic aperture radar imaging geometry.**

$F(k_x, k_y)$ is the two-dimensional spatial Fourier ransform of the complex reflectivity function $(x,y)$ with respect to $x$ and $y$ coordinates, and $(k_u, w)$ is the one-dimensional Fourier transform of he received signal $s(u,w)$ with respect to the ehicle position $u$.

The algorithm involves computing the ne-dimensional Fourier transform of the received ignal, multiplying it by an exponential function, nd then computing the two-dimensional inverse Fourier transform to obtain the complex reflectivity function.

## 6.4 Moving Target Imaging in Synthetic Aperture Radar

The conventional SAR processing is based on the assumption of a fixed object plane on the ground. The presence of moving objects or patches within the imaged area will interfere with the imaging process and degrade the image quality. This is a problem of significant current study. Yang and Mehrdad[28] have recently developed a method for imaging a moving target in a stationary background. The method works with the assumptions that (i) the echoes due to the moving target and the stationary background are separable in the frequency domain, and (ii) the velocity of the moving target is constant.

The imaging algorithm involves the following operations:

1. Separation of echoes due to the moving target and the stationary background, as shown in the block diagram in Fig. 9.

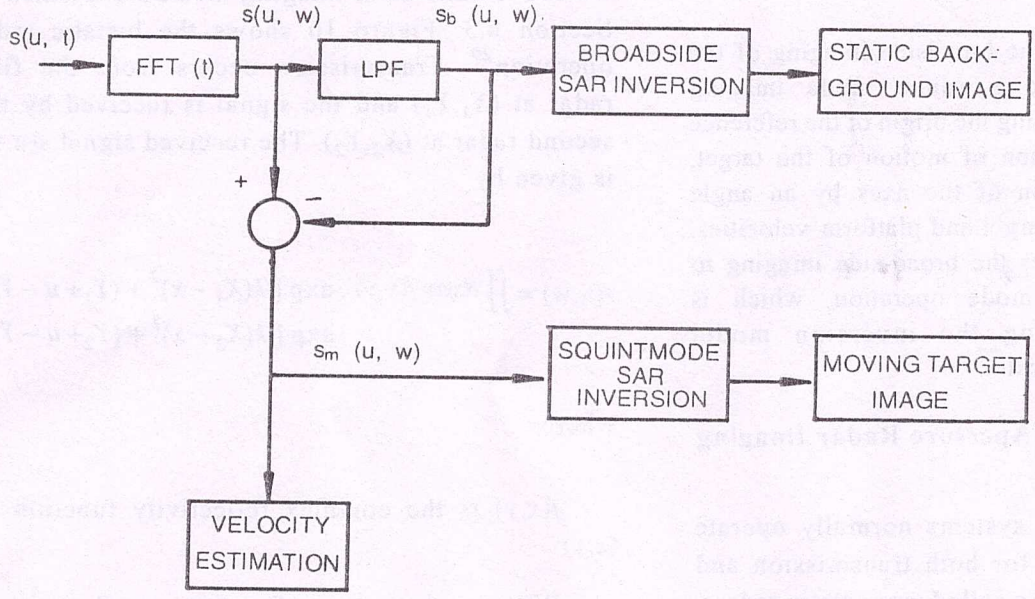


**Figure 9. Block diagram of synthetic aperture radar imaging of a moving target within a stationary background**

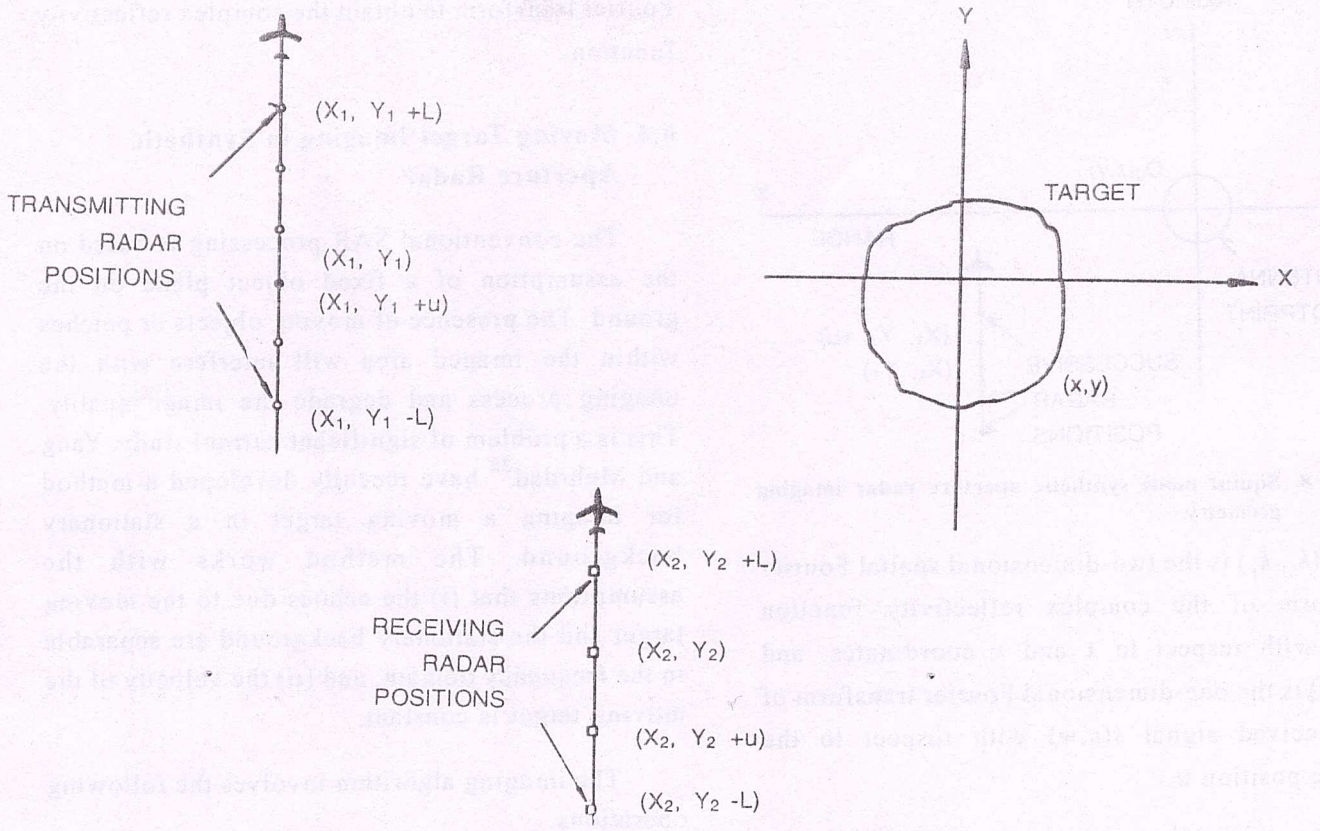


**Figure 10. Bistatic synthetic aperture radar imaging**

2. Estimation of the velocity of the moving target based on the statistical properties of the received signal.

3. Transformation of the broadside imaging of the moving target into a squint mode imaging operation by translating the origin of the reference frame in the direction of motion of the target, followed by rotation of the axes by an angle determined by the target and platform velocities. This process reduces the broad-side imaging to that of a squint mode operation, which is accomplished using the inversion model developed by Soumekh[27]

### 6.5 Bistatic Synthetic Aperture Radar Imaging Model

Conventional SAR systems normally operate from a single platform for both transmission and reception. Such radars are called monostatic radars. Soumekh[29] has developed a method in which the transmitting and receiving radars operate from different platforms. This method is an extension of the monostatic SAR imaging method explained in Section 6.3. Figure 10 shows the bistatic radar operation[29]. Transmission occurs from the first radar at $(X_1,Y_1)$ and the signal is received by the second radar at $(X_2,Y_2)$. The received signal s(u,w) is given by

$$s(u,w) = \iint dxdy\, f(x,y) \cdot \exp\left[jk(X_1 - x)^2 + (Y_1 + u - Y)^2\right] \cdot \exp\left[jk(X_2 - x)^2 + (Y_2 + u - Y)^2\right]$$

where

$f(x,y)$ is the complex reflectivity function at $(x,y)$.

Writing the phase function in the above expression in its integral form, and applying the

method of stationary phase to solve the integral equation, a simple relationship between the two-dimensional spatial frequency transform of the reflectivity function $F(k_x,k_y)$ and the one-dimensional spatial transform of the received signal $S(k_u,w)$ is obtained:

$$F(k_x, k_y) = \exp[-jk(R_1 \cos\Phi_1 + R_2 \cos\Phi_2)]\, S(k_u,w)$$

where

$\Phi_i$ ($i$=1, 2) depends on the spatial coordinates of the transmitting and the receiving radars, and the radar temporal frequency. A two-dimensional inverse Fourier transform of $F(k_x,k_y)$ gives the complex reflectivity function.

The bistatic radar measurements can be used in dynamic object imaging. For a moving scatterer located at $(R,\theta)$ coordinates, the phase correction factor due to its motion is derived[30] and found to be proportional to $\cos^2\theta$. The spectrum of the echo from the point scatterer at $(R,\theta)$ is centered around $k_y = k \sin\theta$. An estimate of $k_y$ obtained using spectral analysis techniques, is used to correct for phase variation due to target motion.

## 7. PRACTICAL SYNTHETIC APERTURE RADAR SYSTEMS

The earliest imaging radar was developed at the Goodyear research facility in Litchfield, Arizona in 1953. This high resolution radar system, which was developed based on Wiley's Doppler beam sharpening concept, operated at 930 MHz with a Yagi antenna having a real beamwidth of 100°. Using Doppler beam sharpening, a synthetic beamwidth of 1° was obtained. By 1958, the University of Illinois developed the first operational motion compensation system, using a Doppler navigator to measure long-term average drifts in conjunction with a gyroscope to correct for short-term yawing of the aircraft. This system was used to develop the fully focused SAR system. In 1957, the Michigan group developed a fully focused SAR system for strip-map imagery using optical correlators.

A single-polarisation X-band SAR system was built by the Environmental Research Institute of Michigan (ERIM) in 1964. Following this, the Jet Propulsion Laboratory (JPL) developed an L-band SAR which was later upgraded to have a simultaneous quad-polarised capability in both L- and C-bands.

The first generation SAR systems were based on optical correlation for SAR compression. The raw data were recorded on photographic films, and subsequently processed in ground facilities involving elaborate and expensive specialised optical processing laboratories. The first on-board digital SAR processor for non-military applications is believed to have been developed by MacDonald-Dettwiler and Associates (MDA) for their imaging system built for the Canadian Center for Remote Sensing in 1979. In 1975, a SAR system was included as part of the Seasat mission for ocean and land mapping. NASA further developed (1986) Shuttle imaging radar (SIR) systems. SIR-A and SIR-B operated in the L- band; SIR-B was a fully digital system. SIR-C, developed in 1990, is a quad-polarised L- and C-band SAR.

The SAR systems have also been effectively used in mapping surfaces of other members of the solar system during space missions. In 1972, NASA initiated the Apollo Lunar Sounder Experiment which was jointly conducted by ERIM and JPL. The mission was to detect subsurface geologic structures to generate a continuous lunar profile, and to map the lunar surface at radar wavelengths. The system used optical holographic techniques for data recording. A high resolution planetary radar, called Magellan, to generate a global map of Venus at approximately 150 m resolution, has been developed by NASA. A second planetary radar under development by NASA/JPL is the Titan Radar Mapper. This instrument will be used in a multi-mode radar designed to measure the surface characteristics of the Saturnian moon Titan as well as to determine the orbit of Cassini, which encircles Saturn and Titan.

Current and future trends in SAR system development indicate a greater use of polarimetric information for object mapping, identification and discrimination. An example is a system currently under development by the Netherlands Agency for Aerospace Programmes. This project, called PHARUS[32], aims to develop a polarimetric C-band aircraft-borne SAR.

## 8. CONCLUSION

In this paper, we have attempted to provide a broad picture of the developments relating to SAR, which has emerged as a powerful tool for surface and subsurface imaging, remote sensing and surveillance. The SAR is now a very well developed device involving many disciplines in systems science, optical and electronic signal processing, and radar system engineering. Also, by its very nature, it involves an interaction between the SAR device and the platform carrying the device. It is an impossible task to cover all those aspects in a brief review paper. We have, therefore, provided a brief outline of the SAR basics, but concentrated on the relatively advanced topics in SAR system theory and signal processing, which are not readily available in previous reviews on the subject.

The SAR is undoubtedly a rapidly evolving field in terms of theoretical understanding, hardware implementation and newer applications. The presentation in this paper must, therefore, be updated with freshly available information as time progresses.

## REFERENCES


1. Skolnik, M.I. Introduction to radar systems. McGraw Hill, New York, 1980.
2. Harger, R.O. Synthetic aperture radar systems: theory and design. Academic Press, New York, 1970.
3. Kovaly, J.J. Synthetic aperture radar. Artech House, Dedham, Mass., 1976.
4. Curlander, J.C. & McDonough, R.N. Synth aperture radar: systems and signal processi John Wiley & Sons, Inc. 1991.
5. Brookner, E. Radar technology. Artech Hou Dedham, Mass., 1977. pp. 251-58.
6. Munson, Jr., D.C. & Visentin, R.L. A sig processing view of strip-mapping synthe aperture radar. *IEEE Trans. Acoust., Spee Signal Processing*, 1989, **37**, 2131-47.
7. Ausherman, D.A.; Kozma, A.; Walker, J.I Jones, H.M. & Poggio, E.C. Developments radar imaging. *IEEE Trans. Aerosp: Electro Syst.*, 1984, **20**, 363-98.
8. Tomiyasu, K. Tutorial review of SAR wit applications to imaging of the ocean surfac *Proc. IEEE*, 1978, **66**(5), 563-583.
9. Sack, M. & Cumming, I. G. Application o efficient linear FM matched filtering algorithm t SAR processing. *IEE Proceedings*, 1985, **132** 45-56.
10. Cafforio, C.; Prati, C. & Rocca, F. SAR real time on-board processing: the polyphase algorithm. *Signal Processing*, 1989, **18**, 397-411.
11. Curlander, J.C.; Wu, C.; & Pang, A. Automated preprocessing of spaceborne SAR data. IGARSS '82, Munich, 1982, FA-1-3-1-6.
12. Li, F.K.; Held, D.N.; Curlander, J.C. & Wu, C. Doppler parameter estimation for spaceborne synthetic-aperture radars. *IEEE Trans. Geosci. Remote Sensing*, 1985, **23**, 47-56.
13. Li, F.K. & Johnson, W.T.K. Ambiguities in spaceborne synthetic aperture radar systems. *IEEE Trans. Aerosp. Electron. Syst.*, 1983, **19**, 389-97.
14. Jin, M.Y. Optimal Doppler centroid estimation for SAR data from a quasi-homogeneous source. *IEEE Trans. Geosci. Remote Sensing*, 1986, **24**, 1022-025.
15. Madsen, S.N. Estimating the Doppler centroid of SAR data. *IEEE Trans. Aerosp. Electron. Syst.*, 1989, **25**, 134-40.

Prati, C. & Rocca, F. Focusing SAR data with time-varying Doppler centroid. *IEEE Trans. Geosci. Remote Sensing*, 1992, **30**, 550-59.

Prati, C.; Rocca, F.; Kost, Y. & Damonti E. Blind deconvolu tion for Doppler centroid estimation in high frequencies SAR. *IEEE Trans. Geosci. Remote Sensing*, 1991, **29**, 934-41.

Chang, C.Y. & Curlander, J.C. Application of the multiple PRF technique to resolve Doppler centroid estimation ambiguity for spaceborne SAR. *IEEE Trans. Geosci. Remote Sensing*, 1992, **30**, 941-49.

Blacknell, D.; Freeman, A.; White, R. G. & Wood, J. W. The prediction of geometric distortion in airborne SAR imagery from autofocus measurements. *IEEE Trans. Geosci. Remote Sensing*, 1987, **325**, 775-82.

Quegan, S. Measurement of geometric distortion in airborne SAR images. Proceedings of the IGARSS'84, 27-30 August, 1984, Strasbourg, France. pp. 595-99.

Wood, J. W. The production of distortion free SAR imagery. Proceedings of the International Conference Radar' 87, 19-21 October 1987, London, UK. pp. 471-73.

Jin, M. Y. & Chialin, W. A SAR correlation algorithm which accomodates large range migration. *IEEE Trans. Geosci. Remote Sensing*, 1984, **22**, 592-97.

Wu, K. H. Extensions to the step transform to accomodate nonlinear range migration and high squint angle. *IEEE Trans. Aerosp., Electron., Syst.*, 1985, **25**, 338-344.

Eichel, P. H.; Ghiglia, D. C. & Jakowatz, C. V. Speckle processing method for SAR phase correction. *Optics Lett.*, 1989, **14**, 1-3.

25. Bamler, R. A Comparison of Range-Doppler and wavenumber domain SAR focusing algorithm. *IEEE Trans. Geosci. Remote Sensing*, 1992, **30**, 706-13.

26. Cafforio, C.; Prati, C. & Rocca F. SAR Data Focusing Using Seismic Migration Techniques. *IEEE Trans. Geosci. Remote Sens.*, 1991, **27**, 194-207.

27. Soumekh, M. A system model and inversion for synthetic aperture radar imaging. *IEEE Trans. Image Processing*, 1992, **1**, 64-76.

28. Yang, H. & Soumekh, M. Blind Velocity SAR/ISAR imaging of a moving target in a stationary background. *IEEE Trans. Image Processing*, 1993, **2**, 80-95.

29. Soumekh, M. Bistatic synthetic aperture radar inversion with application in dynamic object imaging. *IEEE Trans. Signal Processing*, 1992, **39**, 2044-055.

30. Werness, S.A.S.; Carrara, W.G.; Joyce, L.S. & Franczak, D.B. Moving target imaging algorithm for SAR data. *IEEE Trans. Aerosp. Electron. Syst.*, 1990, **26**, 57-67.

31. Blacknell, D.; Freeman, A.; Quegan, S.; Ward, I.A.; Finley, I.P.; Oliver, C.J; White, R.G. & Wood, J.W. Geometric accuracy in airborne SAR images. *IEEE Trans. Aerosp. Electron. Syst.*, 1989, **25**, 241-56.

32. Hoogeboom, P.; Snoeij, P.; Koomen, P.J. & Pouwels, H. The PHARUS project, results of the definition study including the SAR testbed PHARS. *IEEE Trans. Geosci. Remote Sensing*, 1992, **30**, 723-35.

Contributors

**Mr MS Ranga Rao** obtained his ME in Electronics and Communication Engineering from Osmania University, Hyderabad, in 1990. He joined DRDO at the Defence Research & Development Laboratory (DRDL) Hyderabad. His areas of research include: radar signal processing, synthetic aperture radars and image processing techniques.

**Dr PR Mahapatra** received his ME and PhD both from the Indian Institute of Science (IISc), Bangalore. His areas of research include radars, electronic navigational aids, navigation theory, aviation safety problems with particular reference to weather phenomena and air traffic control, and signal processing. He has published over one hundred scientific research papers. He is a fellow of the Institute of Electronics and Telecommunication Engineers (IETE), India and is a professional member of the Institute of Navigation, USA.